◆ Human Brain Mapping 37:20–34 (2016) ◆

Multimodal Description of Whole Brain Connectivity: *A Comparison of Resting State MEG, fMRI, and DWI*

Pilar Garcés,[1] Ernesto Pereda,[2] Juan A. Hernández-Tamames,[3] Francisco Del-Pozo,[1,4] Fernando Maestú,[1,4] and José Ángel Pineda-Pardo[1,5]*

[1]*Laboratory of Cognitive and Computational Neuroscience, Centre for Biomedical Technology, Universidad Politécnica De Madrid, Campus De Montegancedo, Pozuelo De Alarcón, Madrid 28223, Spain*
[2]*Department of Industrial Engineering, Institute of Biomedical Technology (ITB-CIBINCAN), Universidad De La Laguna, Avda. Astrofísico Fco. Sánchez S/N, La Laguna, Tenerife 38205, Spain*
[3]*Department of Electronics Technology, Universidad Rey Juan Carlos, C/Tulipán S/N, Móstoles, Madrid 28933, Spain*
[4]*Biomedical Research Networking Center in Bioengineering, Biomaterials and Nanomedicine (CIBER-BBN), Madrid, Spain*
[5]*CINAC, HM Puerta del Sur, Hospitales de Madrid, 28938 Móstoles, and CEU-San Pablo University, 28003, Madrid, Spain*

Abstract: Structural and functional connectivity (SC and FC) have received much attention over the last decade, as they offer unique insight into the coordination of brain functioning. They are often assessed independently with three imaging modalities: SC using diffusion-weighted imaging (DWI), FC using functional magnetic resonance imaging (fMRI), and magnetoencephalography/electroencephalography (MEG/EEG). DWI provides information about white matter organization, allowing the reconstruction of fiber bundles. fMRI uses blood-oxygenation level-dependent (BOLD) contrast to indirectly map neuronal activation. MEG and EEG are direct measures of neuronal activity, as they are sensitive to the synchronous inputs in pyramidal neurons. Seminal studies have targeted either the electrophysiological substrate of BOLD or the anatomical basis of FC. However, multimodal comparisons have been scarcely performed, and the relation between SC, fMRI-FC, and MEG-FC is still unclear. Here we present a systematic comparison of SC, resting state fMRI-FC, and MEG-FC between cortical regions, by evaluating their similarities at three different scales: global network, node, and hub distribution. We obtained strong similarities between the three modalities, especially for the following pairwise combinations: SC and fMRI-FC; SC and MEG-FC at theta, alpha, beta and gamma bands; and fMRI-FC and MEG-FC in alpha and beta. Furthermore, highest node similarity was found for regions

Additional Supporting Information may be found in the online version of this article.

Contract grant sponsor: Spanish Ministry of Education (National Program FPU); Contract grant number: AP2010-1317; Contract grant sponsor: Spanish MINECO; Contract grant numbers: TEC2012-38453-C04-01 and TEC2012-38453-C04-03; Contract grant sponsor: European Commission; Contract grant number: 612022; Contract grant sponsor: Moncloa Campus of International Excellence (UCM–UPM; P.G.)

*Correspondence to: José Ángel Pineda-Pardo, Centre for Biomedical Technology, Universidad Politécnica de Madrid, 28223 Madrid, Spain. E-mail: joseangel.pineda@ctb.upm.es

Received for publication 21 February 2015; Revised 26 August 2015; Accepted 27 August 2015.

DOI: 10.1002/hbm.22995
Published online 27 October 2015 in Wiley Online Library (wileyonlinelibrary.com).

of the default mode network and primary motor cortex, which also presented the highest hubness score. Distance was partially responsible for these similarities since it biased all three connectivity estimates, but not the unique contributor, since similarities remained after controlling for distance. *Hum Brain Mapp 37:20–34, 2016.*

Key words: functional connectivity; structural connectivity; fMRI; MEG; DWI

INTRODUCTION

Neuroimaging techniques such as magnetoencephalography (MEG) or functional magnetic resonance imaging (fMRI) provide noninvasive, *in vivo* observations of the working brain. While MEG measures coherent neuronal activity at the ms scale, which is mainly generated by postsynaptic currents in apical dendrites [Hämäläinen et al., 1993; Lopes da Silva, 2010], blood-oxygen level-dependent (BOLD) fMRI signals result from the dynamic variations in the ratio of oxy- and deoxyhemoglobin [Ogawa et al., 1992] and fluctuates at a slower temporal scale (∼3s). Although both modalities measure brain activity, they reflect distinct neuronal processes. For instance, incoherent activity or inhibitory spiking, which might be invisible to MEG also induce metabolic changes [Singh, 2012], which in some cases, might even mask coherent activity related metabolism. Despite these differences, MEG and fMRI measures are interrelated. In fact, independent activation studies using MEG or fMRI have obtained converging results in the mapping of cognitive processes [Dale et al., 2000]. Moreover, simultaneous setups recording electrical neurophysiological activity and BOLD fMRI in primates or humans undergoing neurosurgical procedures have established causality between neuronal firing and BOLD fMRI changes [Logothetis, 2003; Mukamel et al., 2005; Singh, 2012]. With simultaneous EEG-fMRI in humans, Laufs et al. [2003] revealed correlations between EEG power and BOLD activity in alpha band (8–12 Hz) and low-beta (17–23 Hz). Using separate MEG and fMRI recordings, Zumer et al. [2010] also observed a correlation between MEG and fMRI signals.

A very important concept in modern neuroscience, which has also been studied with both fMRI and MEG, is that of functional connectivity (FC). It is normally defined as the existence of a statistical relationship between two (or among many) simultaneously recorded signals of brain activity. FC is considered the most plausible mechanism for neuronal transfer of information [Singer and Gray, 1995], and has been widely studied with electrophysiological techniques. However, FC can also be assessed from the correlation between BOLD time series (fMRI-FC), which has recently unveiled large-scale functional networks that are working coordinately even in the absence of an attentional-demanding task [Fox et al., 2006]. Of high relevance is the default mode network (DMN), which consists of a set of regions that deactivate when subjects become involved in an attention-demanding task [Greicius et al., 2003; Raichle and Snyder, 2007]. Interestingly, although their origin is unclear, these networks have been replicated using MEG-FC [Brookes et al., 2011b; de Pasquale et al., 2010; Hipp et al., 2012; Luckhoo et al., 2012], thus proving that these fMRI networks have a neurophysiological basis, especially in alpha and beta bands.

Aside from these so-called resting state networks, whole-brain FC networks can also be computed by partitioning the brain grey matter in a set of regions related to specific anatomical [Fischl et al., 2004; Tzourio-Mazoyer et al., 2002], functional [Power et al., 2011; Shen et al., 2013; Varoquaux and Craddock, 2013; Yeo et al., 2011] or random atlases [Hagmann et al., 2008], and estimating the degree of FC between each pair of regions (or nodes). Such whole-brain networks are useful in the study of brain organization using graph theory analysis [Bullmore and Sporns, 2009; Papo et al., 2014]. Nevertheless, the degree of similarity between fMRI and MEG-FC in such whole-brain networks has been scarcely studied. Only very recently, Tewarie et al. [2014] examined the overlap between fMRI-FC and MEG-FC and found that it was highest in the alpha and beta bands. These authors reproduced both MEG and fMRI-FC using a structural connectivity template, thus suggesting that both FC have a common anatomical basis. In their analysis, they focused on subject average connectivity from different samples, thereby neglecting subject-specific variability.

It is commonly accepted that FC requires a physical path of white matter fibers that enables information transfer. For instance, the corpus callosum is essential for interhemispheric FC [Johnston et al., 2008; Quigley et al., 2003]. Structural connectivity (SC), which quantifies the strength or integrity of these paths, can be non-invasively measured using DWI. The correspondence between SC and fMRI-FC has been studied over the last few years,

Abbreviations

BOLD	blood-oxygenation level-dependent
CSF	cerebrospinal fluid
DMN	default mode network
DWI	diffusion-weighted imaging
EEG	electroencephalography
FDR	false discovery rate
FC	functional connectivity
fMRI	functional magnetic resonance imaging
MEG	magnetoencephalography

especially in large-scale resting state networks. Strong positive correlations are usually found between both SC and fMRI-FC, especially in the DMN [Greicius et al., 2009; Khalsa et al., 2014; van den Heuvel et al., 2009]. However, the dependence between SC and FC is not always clear. For example, Hermundstad et al. [2013] found that the strength of fMRI-FC is explained by the density and length of fibers composing the SC network, and strong SC values relate to strong fMRI-FC, but fMRI-FC can be also found in the absence of reconstructed fibers [Honey et al., 2009; Skudlarski et al., 2008]. Deco et al. [2011] reviewed computational models that predicted large-scale network dynamics relying on the SC. More recently, Goñi et al. [2014] observed that SC-derived measures of information theory predict the strength of fMRI-FC better than computational models or the strength of the connection, and could account for unconnected regions. Altogether, this leads to the idea that FC is constrained by structure in a nontrivial way, and therefore, its estimation can be informed by SC [Hinne et al., 2014; Pineda-Pardo et al., 2014], which leads to a more accurate description of information transfer within the brain.

Depending on the distance between the nodes involved, two types of FC have been discriminated in invasive electrophysiological recordings, namely short-range [Gray et al., 1989] and long-range connectivity [Roelfsema et al., 1997]. In noninvasive recordings, distance constitutes a major confound in the study of brain connectivity. Noninvasive brain mapping techniques are biased by distance because of source leakage (e.g. MEG [Brookes et al., 2012]), head motion during scanning (e.g. MEG and fMRI) [Van Dijk et al., 2012] and uncertainty in the tracking of long fibers (e.g. SC) [Jbabdi and Johansen-Berg, 2011]. Many studies have addressed the contribution of distance in FC and SC, and although a strong inverse relation has been defined between connectivity and interregional distance [Alexander-Bloch et al., 2013; Honey et al., 2009], coupling strength is not solely explained on this variable [Vértes et al., 2012]. We believe that intermodality similarities should explain different organization properties at the short- and the long-range networks. Whereas short-range similarities could be attributed to the hierarchical and modular organization, long-range similarities could be attributed to an integrative topology, which should be commonly explained with the different techniques.

Although much work has been done in the description of SC and FC networks with different imaging modalities, to the best of our knowledge no study has thoroughly evaluated the similarity of SC, fMRI-FC, and MEG-FC networks. In this work, we aim at identifying commonalities and differences at the individual level between the three modalities of brain connectivity described before: SC, fMRI-FC, and MEG-FC. For that purpose, we parcellated the brain of nine healthy subjects in sixty-six cortical regions. Then SC, MEG-FC, and fMRI-FC were estimated between each pair of regions (or nodes) and subsequently, the resulting connectivity patterns (networks) were compared at different scales. Thus, similarity between networks was first studied globally using the Hamming distance. Then, connectivity values were ranked, and intermodality similarity was computed locally for all nodes using a minimum ratio metric. Thirdly, the hubness of each node (i.e. its relevance for the network) was compared intermodality, to study whether the functional centrality of a node is sustained by a structural centrality, and the possible neurophysiological correspondence of the well described SC and fMRI-FC hubs. Finally, we examined to which extent intermodality similarities are biased by distance. For that purpose, we calculated the previous similarity measures for short- and long-range connections separately, by establishing a distance threshold, and identified the contribution of short- and long-range connections to the highest connectivity values.

MATERIALS AND METHODS

Subjects

The sample comprised nine young subjects (five right-handed; four males; mean age: 28.4, S.D.: 2.5), who presented no history of psychiatric or neurological illness. Prior to their enrolment in the study, informed written consent was obtained from all of them, in accordance with the regulations of Fundación CIEN-Fundación Reina Sofía and Centre for Biomedical Technology (Madrid).

MEG Acquisition

Five-minute MEG resting-state recordings were acquired at the Center for Biomedical Technology (Madrid, Spain) using an Elekta Vectorview system with 306 sensors (102 magnetometers and 204 planar gradiometers), inside a magnetically shielded room (Vacuumschmelze GmbH, Hanau, Germany). During the measurements, subjects sat with their eyes closed and were instructed to remain calm and move as little as possible. A Fastrak Polhemus system digitized each subject's head and four coils were attached to the forehead and mastoids, so that the head position with respect to the MEG helmet was determined. Activity in electrooculogram channels was also recorded to keep track of ocular artefacts. Signals were sampled at 1000 Hz with an online filter of bandwidth 0.1-300 Hz. Maxfilter software (version 2.2., Elekta Neuromag) was used to remove external noise with the temporal extension of the signal space separation (tsss) method [Taulu and Simola, 2006].

MRI Acquisition

Each participant was scanned on a 3T General Electric MR scanner (General Electric Healthcare, Farfield, CT), using a whole-body radiofrequency (RF) coil for signal excitation and quadrature 8-channel brain coil for

reception. The acquisition protocol consisted of: (1) high resolution 3D T1-weighted SPGR with TR/TE/flip angle of 9.1ms/4.1ms/10°, FoV = 256 mm, matrix = 256 × 256, slice thickness of 1 mm, voxel size = 1 × 1 × 1 mm^3; (2) six minutes resting-state fMRI scan with Gradient-Echo echo-planar sequence with TR/TE of 1625/27.6 ms, NEX=1, FoV=230 mm, matrix = 96 × 96, slice thickness = 2.4 mm, voxel size = 2.4 × 2.4 × 2.4 mm^3; (3) diffusion weighted images (DWI) in 45 non-collinear encoding directions and a b value of 1000 s/mm^2 with single-shot spin echo echo-planar sequence with TR/TE of 12700/88.3 ms, NEX=2, FoV = 230 mm, matrix = 96 × 96, slice thickness = 2.4 mm, voxel size = 2.4 × 2.4 × 2.4 mm^3, and two additional images with no diffusion sensitization $b = 0$ s/mm^2 (b_0); and (4) two sets of two gradient echo images (fMRI and DWI spatial resolution) with different echo times, 6.5 and 8.5 ms, TR = 600 ms and flip angle = 45°. In addition during the fMRI acquisition, subjects' cardiac pulse signals were recorded using a pulse-oximeter placed on the left index finger. Respiration was measured with a pneumatic belt placed around the subject's abdomen.

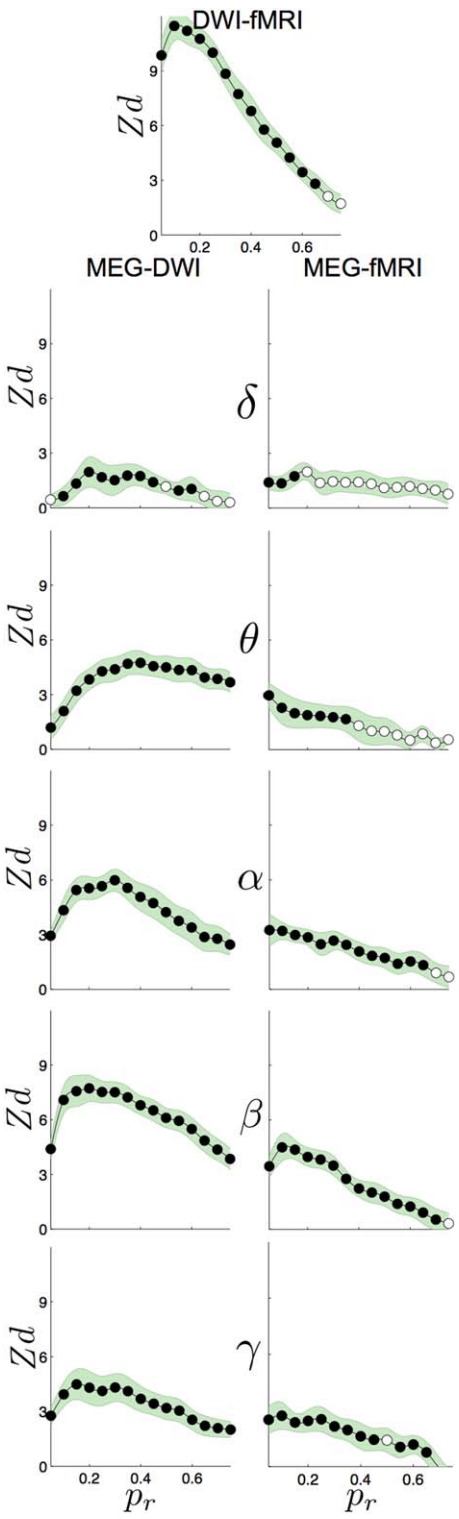

Regions of Interest

Sixty-six cortical regions of interest (ROIs) were used to compute connectivity in all three modalities (MEG, fMRI, and DWI). These ROIs were defined in the individual's T1 volume, using Freesurfer software (version 5.1.0) and its cortical parcellation [Desikan et al., 2006] (see supplementary Figure 1 and Supporting Information Table I for a description of the cortical regions and abbreviations). For MEG, a 4 × 4 homogenous transformation matrix from T1 space to MEG coordinate system was obtained by manually matching the headshape digitalized in the MEG system and the skin extracted from the T1 volume.

MEG Functional Connectivity

MEG source reconstruction

First, ocular, jump and muscular artefacts were identified and located in the 5-minute resting state recordings, using the FieldTrip toolbox [Oostenveld et al., 2011]. Artifacted samples (with 1 second padding to avoid contamination to segments surrounding artifacts) were not used

Figure 1.

Global network similarity. Hamming distances between connectivity matrices are plotted for each pair of modalities and frequency band as a function of p_r (the proportion of non-zero connections in the connectivity matrices). Distances are z-scored with a surrogate dataset, and positive values of higher amplitudes indicate stronger similarities. Central line and green shading indicate the subject average and the standard deviation over subjects, respectively. Filled black circles mark significantly small distances, when compared with the surrogate dataset (false discovery rate, $q = 0.01$). [Color figure can be viewed in the online issue, which is available at wileyonlinelibrary.com.]

for the source and connectivity analysis. However, all five-minute resting state data were used for bandpass filtering to avoid edge artifacts. Data were filtered into five frequency bands of interest: delta (2–4 Hz), theta (4–8 Hz), alpha (8–12 Hz), beta (12–30 Hz) and gamma (30–45 Hz) with finite impulse response (FIR) filters of order 1000.

Source reconstruction was performed with linearly constrained minimum variance beamformer [Van Veen et al., 1997] separately for each frequency band. For each subject and frequency band, the covariance matrix over all nonartifacted time points was used to compute the spatial filter's coefficients, which were then applied to the MEG sensor data, thereby obtaining both a time series and a source location. To avoid mixing MEG sensors with different sensitivities or resorting to scaling, only magnetometers were used for this source reconstruction step. We must note, however, that gradiometer information is indirectly present as both magnetometers and gradiometers were used in the tsss filtering.

Functional connectivity

Before computing the FC values, a leakage correction was performed in the time domain to control for volume conduction, as suggested in [Brookes et al., 2012; Maldjian et al., 2014]. Then, the amplitude of the source time series was extracted with a Hilbert transform, and smoothed with a boxcar filter of 1 second width. Correlation between these amplitudes constituted the MEG-FC estimate. For each ROI, a representative time series was chosen as the time series that presented the highest average correlation with the other sources of the ROI, yielding a 66×66 connectivity matrix.

fMRI Functional Connectivity

We employed FSL to pre-process the fMRI time-series. Slice timing correction tool was used to correct the different timing of the slice's voxels. MCFLIRT tool was used to realign the fMRI scans, using as reference the fMRI volume in the middle of the series. Then BET [Smith, 2002] was employed to create a brain mask on the average fMRI volume, and this mask was applied across volumes. We built an inhomogeneity fieldmap using the acquired gradient echo images; and using FUGUE-FSL, fMRI images were unwarped to correct the EPI artifacts due to the magnetic field inhomogeneities. We applied a Gaussian smoothing of 5 mm full-width half-maximum to the fMRI volumes and finally a high-pass filter of 0.01 Hz. Binary white matter (WM) and cerebrospinal fluid (CSF) masks were created by applying a 0.8 threshold to the probability maps extracted from FAST-FSL. WM and CSF regressors were obtained by averaging the fMRI time-series across the masks. Global signal regressor was estimated by averaging all fMRI time series within the brain mask. In addition to these regressors, we used RETROICOR [Glover et al., 2000] to model the cardiac and respiratory contributions to the fMRI noise. Physiological signals were sampled at each of the fMRI volumes. Pulse-oximeter waveforms were used to compute the cardiac phase of each fMRI sample. Together with the cardiac phase, the respiratory phase was estimated following the method described in [Glover et al., 2000]. The cardiac and respiratory noise signals were modeled as sine and cosine basis functions of a Fourier series of order two, ending with eight regressors.

Time-series were averaged across voxels in each of the 66 regions. All 11 regressors (WM, CSF, global, and RETROICOR), together with the six residuals of the fMRI series realignment were regressed out from the 66 regional time-series, using linear least squares. These residuals of this regression were band-pass filtered [0.01–0.09 Hz] using an infinite impulse response Butterworth filter of order 10. Functional connectivity metric was estimated with the Pearson correlation coefficients between the 66 ROI time-series.

Structural Connectivity

DWI images were pre-processed using FMRIB's Diffusion Toolbox (FDT). Correction for motion and geometrical distortion due to eddy currents was performed with the *eddycorrect* tool in FDT, taking as reference image the average of the three b_0 volumes, which were previously realigned using a linear affine transformation. Rotation matrices from the motion correction were also applied to the diffusion gradient directions. Non-brain tissue from the average b_0 image was removed using FMRIB's Brain Extraction Toolbox (BET) [Smith, 2002]. The obtained brain mask was applied to the rest of the DWI images. We built the inhomogeneity fieldmap using the two gradient echo images with different echo times. By means of the FUGUE-FSL, we used the fieldmap image to unwarp the DWI images to correct (in part) the geometric distortion and signal loss because of the magnetic field inhomogeneities. Estimation of the local probability distribution of fibre direction at each voxel was estimated using bedpostx [Behrens et al., 2007]. Fibre populations for each seed volume were estimated with Probtrackx 2.0 [Behrens et al., 2007]. 66 seed volumes were defined, i.e. one per ROI. For each voxel in the seed volume, 5000 streamlines were initiated. The structural connectivity between two regions *(i,j)* was computed as the sum of the streamlines seeded in one region i that ended in region j. Since the connectivity from i to j, is not necessarily the same than that from j to i, we defined a unique connectivity between i and j, i.e. SC_{ij}, as the average of both estimates.

Comparison Between Modalities

To have a comprehensive picture of the similarities between the networks in each modality, MEG-FC, fMRI-FC and SC networks were compared at different scales: from the local level, by analyzing the features of each

single node, to the global level, by estimating the distances between the whole networks. This was performed separately for each pair of modalities and each MEG frequency band (MEG-FC for delta, theta, alpha, beta and gamma bands, broadband fMRI-FC and SC). In the following, networks are defined as graphs, consisting in $N = 66$ nodes (or regions) connected with edges whose weights are defined by functional or structural connectivity values.

Global network similarity

To first evaluate the linear dependence between SC, fMRI-FC and MEG-FC connectivity values, Spearman's correlation coefficients ρ were computed between all pairs of modalities, using all 66*65/2=2145 links. This was performed both for individual subjects and for the subject-average connectivity matrix. Additionally, to account for the effect of distance between ROIs, correlations were calculated using the Euclidean distance between ROI centers as a covariate. ROI centers were computed by averaging the coordinates of all voxels belonging to the ROI.

To further assess whole-network similarity, binary connectivity matrices were obtained by applying a fixed density threshold to the weighted data so that their values were set to zero for a fraction (1-p_r) of their links with lower values, and to 1 for the remaining links, with p_r ranging between 0.05 and 0.75 in steps of 0.05. Then, the Hamming distance between these binary matrices of each modality was computed, yielding a distance metric $d(k,l,p_r)$ for each pair of modalities k and l and p_r value. Hamming distance is defined as the number of links that differed between two binary matrices, i.e., in our case, $d(k,l,p_r)=0$ if the p_r strongest links in modality k are exactly the same as those in modality l, whereas it attains its highest possible value if there are no matches between them.

To assess the statistical significance of these distances, 2000 surrogates were constructed from each original connectivity matrix. For fMRI-FC and MEG-FC matrices, surrogate matrices were obtained with the Hirschberger-Qi-Steuer algorithm [Hirschberger et al., 2007], as implemented in [Zalesky et al., 2012]. These surrogate networks maintain three properties of the original FC matrices: the mean and variance of the off-diagonal elements and the mean of the diagonal elements. Surrogate matrices for SC were obtained with the Maslov-Sneppen randomization [Maslov and Sneppen, 2002] which preserves the original node degree. Hamming distances were then computed for these surrogate networks, yielding a set of surrogate distances $d_{rand}(k,l,p_r,s)$, $s = 1,2,\ldots,2000$ for each value of the (k,l,p_r) triplet. Then, the original distance metrics were z-scored:

$$Z_d(k,l,p_r) = -\frac{d(k,l,p_r) - mean_s(d_{rand}(k,l,p_r,s))}{std_s(d_{rand}(k,l,p_r,s))} \quad (1)$$

were $mean_s$ and std_s represent, respectively, the mean and standard deviation of the distances for the surrogate networks. The smallest the distance between the original networks when compared to the distance between surrogate networks, the higher Z_d. This analysis was performed for each subject separately, and also for the subject average, in order to estimate a p-value of the distance for each (k,l,p_r) combination. The p-value is defined non-parametrically as the proportion of surrogates that yielded lower distances than the original dataset. p-values were then corrected for multiple comparisons with false discovery rate (FDR) ($q = 0.01$) [Benjamini and Yekutieli, 2001].

Node similarity

Connectivity values between each pair of modalities k and l were compared using a similarity metric. First, connectivity values, which are the links connecting two ROIs i and j, were replaced by their rank values, $r(k,i,j)$, within the connectivity matrix of each modality. Then, the similarity of each link (i,j) between the pair of modalities (k,l) was assessed with the minimum ratio [Goshtasby, 2012]:

$$s(k,l,i,j) = \min\left\{\frac{r(k,i,j)}{r(l,i,j)}, \frac{r(l,i,j)}{r(k,i,j)}\right\} \quad (2)$$

The closer this ratio gets to 1, the more similar the link (i,j) is between modalities k and l. Then, the values of $s(k,l,i,j)$ were averaged per each node, yielding an average similarity measure per node i and modality pair (k,l). As in "Global network similarity", statistical significance in the similarity of the node was assessed using surrogate networks, and the corresponding p-values were corrected for multiple comparisons using the FDR algorithm.

Hubness similarity

The hubness of each node of the networks was estimated using a rank average of network centrality measures [Betzel et al., 2014a]. Briefly, for all connectivity matrices, two centrality measures were calculated: node strength (S_i), and eigenvector centrality (ec_i), as implemented in the Brain Connectivity toolbox [Rubinov and Sporns, 2010] (see Supplementary material for further details on the estimation of these measures). Then, each of these measures was rank-transformed, so that integer numbers from 1 to 66 were assigned to each node (ROI). Node hubness was then calculated as the average of these two rank-transformed measures.

Distance contribution

To evaluate whether similarities between connectivity matrices from different modalities are specific of short- or long-range interactions, the analyses described in sections "Global network similarity" and " Node similarity" were repeated separately for short and long distance connections. Links connecting regions whose centroids were separated by 4 cm or less (Euclidean distance) were classified as short range ones and the remaining ones were classified

TABLE I. Spearman's ρ correlation coefficient between connectivity values for each pair of modalities

			fMRI						DWI				
			DWI	MEG delta	MEG theta	MEG alpha	MEG beta	MEG gamma	MEG delta	MEG theta	MEG alpha	MEG beta	MEG gamma
Raw links	Individual subjects	mean	0.20	0.04	0.04	0.06	0.07	0.04	0.04	0.16	0.17	0.25	0.12
		SE	0.02	0.02	0.02	0.02	0.02	0.02	0.02	0.02	0.02	0.02	0.02
	Subject average		0.28	0.07	0.07	0.16	0.16	0.13	0.14	0.36	0.39	0.45	0.33
Distance covariate	Individual subjects	mean	0.10	0.02	0.01	0.01	0.00	0.00	0.00	0.10	0.05	0.12	0.03
		SE	0.02	0.01	0.01	0.01	0.02	0.02	0.02	0.02	0.02	0.02	0.02
	Subject average		0.14	0.01	−0.03	0.02	0.02	0.00	0.03	0.23	0.17	0.24	0.12

Correlations were computed for individual subjects (reported as mean and standard error (SE)), and for the average connectivity matrix. In the three bottom rows, the inverse distance between ROI centers was included as an additional variable for the computation of ρ.

as long-range. In addition, to test frequency band specificity for the short- and long-range connectivity, as suggested by [Buzsaki, 2006], we represented the probability density of links versus Euclidean distance for different network densities ($p_r = 0.05$, 0.1, 0.2, 0.3).

RESULTS

Global Network Similarity

Connectivity values were positively correlated (Spearman rank-order correlation ρ) between modalities (Table I). The highest correlations were found for DWI-MEG in theta, alpha and beta (ρ =0.33–0.45), and moderate correlation for fMRI-DWI (ρ =0.28). Correlations for fMRI-MEG were however much smaller for all frequency bands (ρ =0.07–0.16). As distance may bias connectivity values, an analog correlation analysis was performed including the inverse distance between nodes (or ROI centroids). As expected, correlation values decreased considerably for all modality pairs, although the frequency bands with the highest correlation remained unchanged. Highest correlation values were found for DWI-MEG in theta, alpha and beta (ρ =0.17−0.24).

The Hamming distance between binary connectivity matrices was significantly small ($q = 0.01$, FDR corrected) for all pairs of modalities for at least three p_r values, as shown in Figure 1. The highest Z_d values, which indicate the most similar modalities, corresponded to the pair fMRI-DWI at the lowest p_r values (0.05–0.20) and the beta MEG-DWI at intermediate p_r values (0.10-0.40). Considerably small distances ($Z_d > 3$) were also obtained for theta, alpha and gamma MEG-DWI and beta MEG-fMRI. For theta, alpha and gamma MEG-fMRI, Hamming distances were also significantly small, but exhibited smaller Z_d values than the previously commented modality pairs. In contrast, the largest distances, corresponding to the most different modalities, were obtained between delta MEG with DWI and fMRI. Additionally, analogous distances were computed by varying p_r separately in all modalities. The results are shown in Supporting Information Figure S2, and are in line with the previously described results which were obtained by comparing networks of the same density. In fact, strongest similarities were found for DWI-fMRI, especially at low densities, and DWI- MEG theta, alpha and beta at intermediate densities. The fMRI- MEG comparison also reached high Z_d values for alpha and beta at low fMRI densities ($p_r < 0.15$) and intermediate MEG densities ($p_r = 0.10$–0.3).

Node Similarity

Similarity of each node across modalities was further quantified using the minimum ratio metric introduced in Eq. (2). The results for this index indicated a similar organization of the functional/structural networks in all three modalities. To evaluate the role of the different regions, average similarity per ROI (or node) was computed (Fig. 2). Although significant values were obtained in all comparisons (FDR corrected, $q = 0.05$), similarity values differed between pairs of modalities. The highest values (>0.6) were obtained for MEG-DWI in theta to gamma. The highest similarities were found in the precuneus, the superior and inferior parietal, posterior cingulate and superior frontal ROIs. Similarity values were generally lower for DWI-fMRI and MEG-fMRI, and the 0.6 threshold was not exceeded for any ROI. For the former case (DWI-fMRI), posterior and anterior cingulate, cuneus, superior temporal and lateral orbitofrontal presented the highest similarities. For the latter, the highest similarities were reached in the beta band, although for all frequency bands, some ROIs achieved significant similarities. Highest values were found in posterior and anterior cingulate, cuneus, several temporal ROIs and in the paracentral gyrus. Nodal similarity values can be found overlaid in the brain surface in Supporting Information Figure S3.

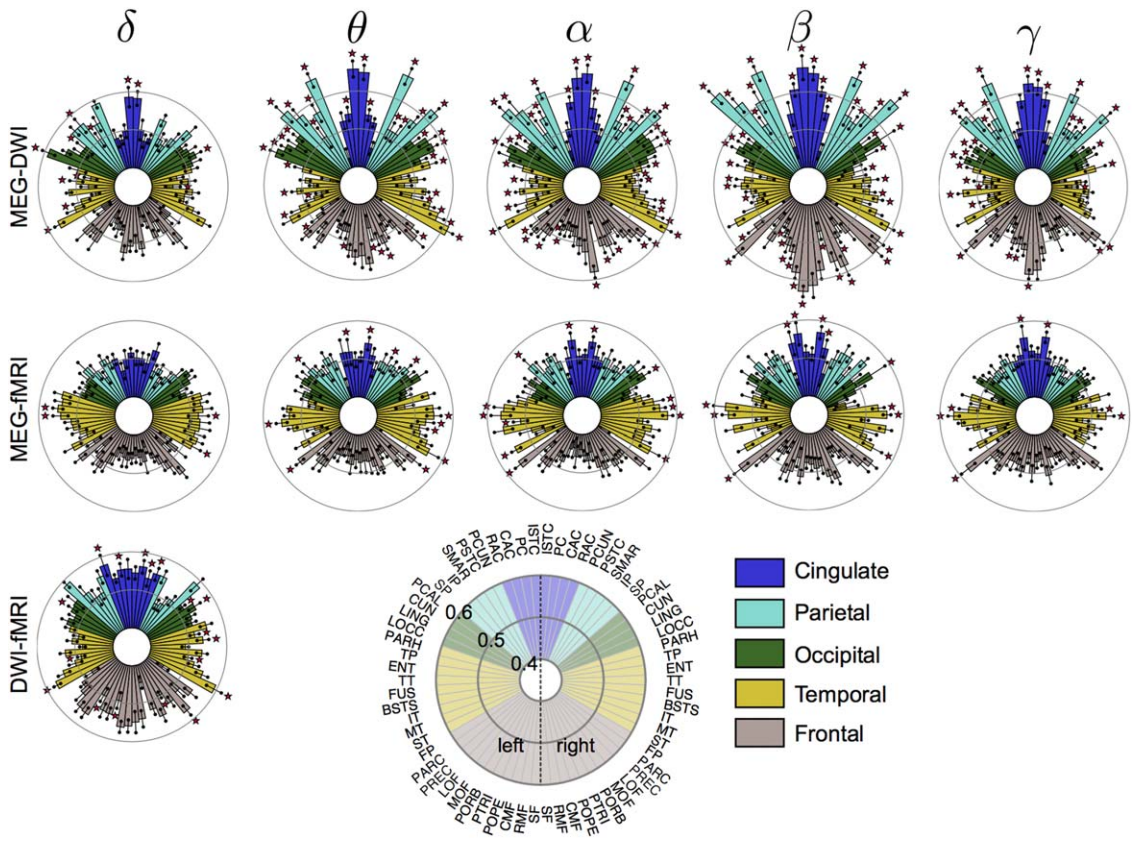

Figure 2.

Node similarity. The average node similarity $\langle \boldsymbol{s}(\boldsymbol{k}.\boldsymbol{l},\boldsymbol{i},\boldsymbol{j})\rangle_{\boldsymbol{j}=1,\ldots,\boldsymbol{N}}$ for each pair of modalities, node and frequency band is displayed in a circular plot. Thirty-three nodes (or regions of interest) per hemisphere are spread in bars over 180°. The bar length indicates the value of the node similarity. ROI labels and scale are shown in the bottom circle, and colors illustrate whether nodes belong to cingulate, parietal, occipital, temporal, or frontal lobe. Error bars represent standard deviation over subjects, and stars highlight significant similarities (false discovery rate, $q = 0.05$). The ordering of the ROIs can be found in the lower disk. Correspondence between codes and full-length names can be found in Supporting Information Table S1. [Color figure can be viewed in the online issue, which is available at wileyonlinelibrary.com.]

Hubness Similarity

Hubness was computed for each connectivity matrix, yielding a hubness rank for each node or ROI. Then, these ranks were correlated between each pair of modalities to test for similarities between them. As shown in Table II, correlations were significant for five combinations: DWI-fMRI, beta- and gamma- MEG-DWI, and beta- and gamma-MEG-fMRI. Among them, DWI-fMRI and beta-MEG-DWI showed the strongest correlations ($\rho = 0.38$ and 0.42 respectively). Further examination of the scatter plots of the hubness provided information on the role of specific ROIs (Fig. 3). In general, the highest hubness values were found in parietal ROIs, while temporal ROIs presented the lowest values. In particular, bilateral precuneus, inferior parietal, precentral and supramarginal regions were among the 33% ROIs with highest hubness for these four modalities (DWI, fMRI, beta-MEG, gamma-MEG). Conversely, weakest hubness were obtained in lateral orbitofrontal, parahippocampal, pars orbitalis, rostral anterior cingulate, frontal pole, entorhinal, transverse temporal and temporal pole ROIs.

Distance Contribution

To examine the relation between distance and SC and FC values, we represented in Figure 4 the probability density of the Euclidean distance of a fraction p_r of the strongest links (0.05, 0.1, 0.2, 0.3) in each network separately (or Supporting Information Fig. S8 for cumulative probabability). For low p_r, connectivity values were shifted towards small distances, so that lower distances related to higher SC and FC. This trend was more pronounced for SC and for MEG-FC from theta to gamma, although it was also present in fMRI-FC and delta MEG-FC.

TABLE II. Correlation between node hubness, strength, and eigenvector centrality for each pair of modalities

		fMRI						DWI				
		DWI	MEG delta	MEG theta	MEG alpha	MEG beta	MEG gamma	MEG delta	MEG theta	MEG alpha	MEG beta	MEG gamma
							Hubness rank					
Individual subjects	Mean	−0.14	0.12	0.03	0.07	0.02	−0.07	−0.04	0.08	0.11	0.23	0.15
	SE	0.13	0.18	0.24	0.17	0.14	0.17	0.12	0.18	0.20	0.12	0.15
Subject average	ρ	0.38	0.03	0.27	0.21	0.29	0.32	−0.32	0.05	0.01	0.42	0.31
	p-value	0.0014*	0.79	0.027*	0.091	0.019*	0.0078*	0.0089*	0.72	0.96	0.0005*	0.010*
							Strength					
Individual subjects	Mean	−0.14	0.12	0.03	0.06	0.02	−0.07	−0.03	0.09	0.12	0.23	0.15
	SE	0.13	0.18	0.24	0.17	0.13	0.16	0.11	0.18	0.19	0.12	0.14
Subject average	ρ	0.46	0.02	0.27	0.20	0.28	0.32	−0.06	0.18	0.12	0.34	0.30
	p-value	0.0001*	0.86	0.031	0.12	0.021*	0.0081*	0.60	0.15	0.32	0.0052*	0.016*
							Eigenvector centrality					
Individual subjects	Mean	−0.13	0.12	0.03	0.07	0.03	−0.07	−0.05	0.07	0.09	0.24	0.15
	SE	0.14	0.18	0.24	0.17	0.14	0.17	0.13	0.19	0.21	0.13	0.16
Subject average	ρ	0.27	0.04	0.28	0.22	0.29	0.33	−0.51	−0.11	−0.14	0.40	0.27
	p-value	0.026*	0.74	0.025	0.071	0.018*	0.0080*	<0.0001*	0.36	0.28	0.0010*	0.030*

*Denote significant p-values after FDR correction, $q = 0.05$

For each subject and measure, the Spearman correlation was calculated, and mean and standard error (SE) over subjects are displayed. The same calculations were performed for the average connectivity matrix, and Spearman correlation coefficients are indicated along with their p-values.

To inspect the contribution of short- and long-range connections to the similarities between modalities, the previous analyses were carried out for short and long-range connections separately. Firstly, at the global network level, similarities were not significant for short range connections (Supporting Information Fig. S4), in all comparisons, except for DWI-fMRI. In addition, there are some contributions of the strongest connections to the similarities between MEG-fMRI in delta to theta bands. Long-range connections, however, were significantly similar between modalities and produced results akin, but with lower significance, to those obtained for the whole network (Supporting Information Fig. S5). This indicates that the global scale similarities between modalities evidenced with thresholded networks are mainly because of long-range connections between the nodes. Secondly, at the level of individual nodes, significant similarities were obtained both for short- and long-range connections, as shown in Supporting Information Figures S6 and S7. For short-range connections, the highest similarities were found in occipital ROIs for MEG-fMRI and parietal ROIs for MEG-DWI. For long-range connections, node similarities resembled the ones obtained with the whole network, and the highest values were obtained for MEG-DWI in theta, alpha, beta and gamma in parietal, frontal and cingulate ROIS and for MEG-fMRI in cingulate and temporal ROIs.

DISCUSSION

In this work, we studied the commonalities between SC and resting-state FC networks extracted with three different imaging modalities: DWI, MEG, and fMRI. For each subject and modality, we computed connectivity matrices between 66 cortical ROIs by using standard analysis techniques: probabilistic tractography for DWI, correlations between BOLD signals for fMRI and envelope correlation for MEG. MEG-FC was computed separately for delta, alpha, beta and gamma frequency bands. Then, we analyzed the similarities between the corresponding structural and functional networks at three different levels. First, we estimated the distance between the global networks of all modalities, and found that they were significantly similar, especially DWI-fMRI and DWI and alpha-, beta- and gamma-MEG. Second, we added spatial resolution by estimating similarities at the regional level, and found that it was highest for the previous pairs of modalities, and especially in parietal, cingulate and frontal ROIs. Third, we explored similarities in the hubness of each ROI, by correlating a hubness aggregated measure. We found significant correlations for all pairwise combinations between DWI, fMRI, and beta and gamma MEG networks. In particular, we found highest hubness in parietal ROIs and lowest values in temporal ROIs. Overall, this indicates that SC, fMRI-FC and MEG-FC networks are related, but it does not imply that they represent the same phenomena or that they can be used interchangeably. Instead, they offer complementary information and provide different insights into brain functioning.

Similarities Between Structural and Functional MRI

Previous studies had already observed that fMRI-FC is shaped by SC [Greicius et al., 2009]. In fact, large-scale

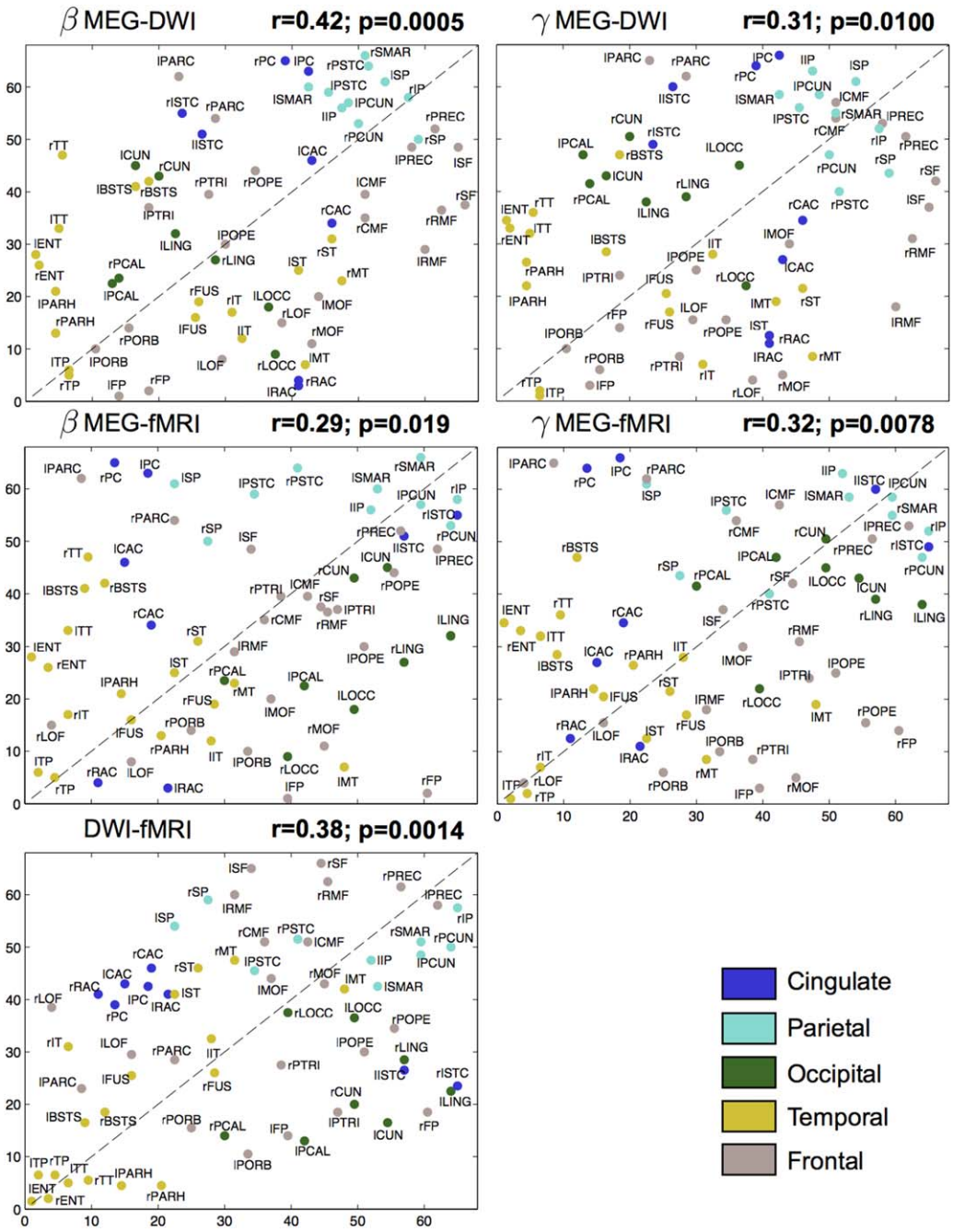

Figure 3.

Hubness correlation. Scatterplots of hubness rank are plotted for DWI-SC, fMRI-FC and beta and gamma MEG-FC. Vertical (horizontal) axis correspond to the first (second) modality in the figure title. Each ROI is plotted as a dot, accompanied by its code. Correspondence between codes and full-length names can be found in Supporting Information Table S1. Dots color illustrate whether nodes belong to cingulate, parietal, occipital, temporal, or frontal lobe. Correlation between hubness rank and its corresponding *p*-value are indicated on the top of each scatterplot. The dashed line corresponds to the identity line $y = x$. [Color figure can be viewed in the online issue, which is available at wileyonlinelibrary.com.]

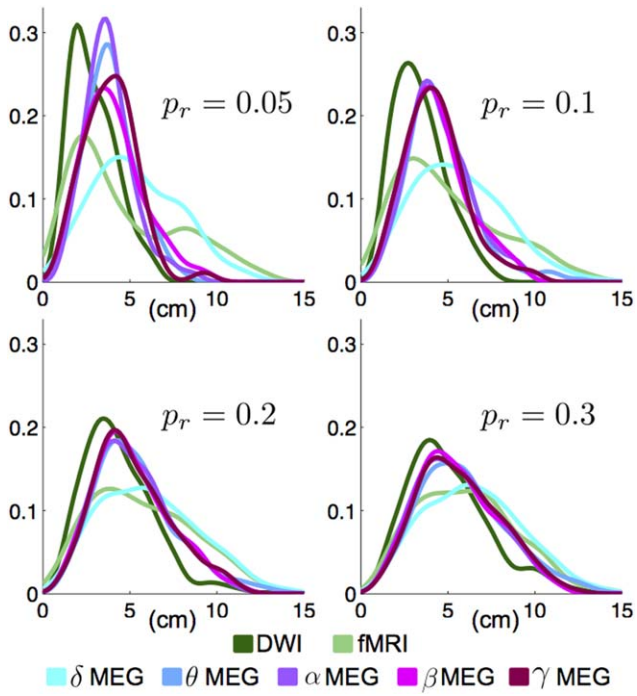

Figure 4.

Distance density of the strongest connections. For each modality separately, the fraction p_r of the strongest links is selected and the probability density of these links is estimated. [Color figure can be viewed in the online issue, which is available at wileyonlinelibrary.com.]

resting-state fMRI networks are supported by structural connections that can be identified using DWI [van den Heuvel et al., 2009]. If these structural connections are weakened or deleted, the resulting functional connectome is strongly altered [Johnston et al., 2008; Quigley et al., 2003]. Our findings contribute to the description of this synergy by suggesting that, when characterizing whole-brain connectivity, the strongest connections are the largest contributors to similarities between fMRI-FC and SC. In fact, the distance between both networks decreased with increasing network sparsity. Similar results were identified by Honey et al. [2009], who suggested that strong SC drives strong fMRI-FC.

At the node level, we found the strongest similarities between SC and fMRI-FC networks for the posterior and anterior cingulate and the precuneus, which are core nodes of the DMN [Greicius et al., 2003]. This is in line with previous studies, which found high correlations between SC and fMRI-FC within the DMN [Hagmann et al., 2008; Honey et al., 2009; Khalsa et al., 2014] and highlighted the prominent role of DMN regions in the agreement between SC and fMRI-FC [Horn et al., 2013; Skudlarski et al., 2008].

Furthermore, the hubness of each node was also similar between SC and fMRI-FC, and regions with the highest hubness generally also presented great similarity measured with the minimum ratio. Skudlarski et al. [2008] first identified this trend, finding that there was greater agreement between SC and fMRI-FC for regions showing strong overall connectivity. Achard et al. [2006] previously identified hubs for fMRI-FC. They classified brain regions as either heteromodal/unimodal association cortex, primary cortex, limbic cortex, and paralimbic cortex [Mesulam, 2010] and located hubs in heteromodal association and primary cortices, whereas limbic and paralimbic regions were generally more peripheral. We also found that paralimbic regions had lower hubness, both for SC and for fMRI, with exception of the isthmus of the cingulate, which showed a large hubness in fMRI-FC. In both modalities, regions from the parietal and the prefrontal association cortices presented a high hubness. These regions, including medial orbitofrontal gyrus, superior frontal, inferior parietal and precuneus, that form part of the DMN, are thought to belong to the brain network core [Hagmann et al., 2008].

MEG Spectral Similarities

Here too, recent publications have demonstrated that FC-MEG/EEG are to some extent related to the underlying structural connections [Cabral et al., 2014; Chu et al., 2014, Tewarie et al., 2014]. In the present work, we found strong similarities between MEG-FC and SC for all frequency bands at all the considered levels: whole network, node, and hubness. Highest similarities were found in the beta band, although strong associations were also present in theta, alpha, and gamma. In a bimodal EEG/DWI study, Chu et al. [2014] found agreement between global FC and SC, particularly in fast frequency bands, albeit these authors did not provide any spatial information. In turn, Cabral et al. [2014] observed that MEG-FC and simulated MEG-FC from SC were strongly correlated in theta, alpha and beta bands. Overall, all these results suggest that MEG-FC in these frequency bands is a good representation of the underlying SC.

At the node scale, we found that many regions presented similar patterns of connectivity between SC and MEG-FC in theta, alpha, beta and gamma frequency bands. Invariably in all frequency bands, inferior parietal, precuneus, posterior and isthmus cingulate showed the strongest intermodal agreement. This indicates that the similarity between SC and MEG-FC from regions of the DMN to the rest of the brain is higher than from other regions to the rest of the brain. This was however not the case for the anterior part of the DMN (anterior cingulate), although some frontal regions presented high similarity between SC and MEG-FC, (i.e. superior frontal, rostral medial frontal, precentral, paracentral). This could derive from the fact that the frontal regions have lower signal-to-noise ratio in MEG, or from the atlas choice, which could influence network topology [Zalesky et al., 2010].

In line with previous studies [Brookes et al., 2011b; de Pasquale et al., 2010; Hipp et al., 2012], similarities between MEG and fMRI were evident in the theta, alpha, beta, and gamma bands. On the contrary, delta presented smaller similarities. Similarities were therefore higher for the faster frequency bands (>8 Hz), although we note that the amplitudes of these faster rhythms oscillate at a slower rate (~1 Hz). Moreover, cingulate, occipital, and temporal regions stuck out as the ones where the FC of both neuroimaging modalities were most similar, especially in the beta band. This partially agrees with a previous study [Tewarie et al., 2014], which reported highest overlap between fMRI-FC and MEG-FC both for parietal and occipital regions in alpha and beta bands. In our work, occipital regions presented rather moderate similarities when considering whole-brain networks, although high values were found when restricting the analysis to short-range connections.

Role of Distance

Previous studies highlighted that distance influences connectivity values [Achard et al., 2006; Honey et al., 2009], although their variability cannot be explained by distance alone, as shown by the existence of strong long distance connections [Vértes et al., 2012]. In our work, for all three modalities analyzed, high SC and FC values were shifted towards small distances, indicating high structural and functional coupling between close regions. This effect was stronger for SC and for MEG-FC from theta to gamma. In fact, we found (Table I) that the high correlation between SC and MEG-FC decreased when including distance in the correlation model. This result indicates that SC and MEG-FC are clearly biased by distance, yet similarities between connectivity values in these two modalities do not result exclusively from it, since correlations remained strong even after correcting by the effect of distance.

We further explored the role of distance in the topology of brain connectivity networks by analyzing whether this parameter influenced the similarities between connectivity networks from different modalities at both the local and the global scale. Thus, we repeated the similarity analysis for short- and long-range connections separately. When considering long-range connections, the z-scored Hamming distance Z_d between SC and MEG-FC increased to a nonsignificant level for delta, but remained small for theta, alpha, beta and gamma bands. When comparing fMRI-FC and MEG-FC, long-range connections were only similar for beta and gamma bands. However, for short-range connections, we did not find any significant similarity at the global level between MEG-FC and either SC or fMRI-FC for any frequency band. This could be due to the fact that, despite using a MEG FC measure that is insensitive to source leakage, short-range FC could not be accurately estimated with MEG. This could seem surprising, since slower brain oscillations are usually associated with global processing while fast oscillations in beta and gamma bands are usually found to be limited to more restricted areas [Knyazev, 2012; Lopes da Silva, 2013]. Contrarily, Z_d between SC and fMRI-FC was significantly big for both short- and long-range connections.

At the node level, when one only considers long-range connections most of the findings for the similarity between fMRI-FC and SC were preserved, including those for the DMN. Similarities between SC and MEG-FC were preserved for long-range connections for theta to gamma. For short-range connections, however, the similarity profiles were strikingly modified. While similarities decreased in cingulate, temporal, and frontal regions, strong similarities emerged in occipital regions. These significant similarities in occipital regions for short-range connections were also present when comparing fMRI-FC and MEG-FC for theta, alpha, and beta bands. Strong similarities in occipital regions were also found between SC and fMRI-FC, possibly indicating that these regions are forming a modular short-range subnetwork

Limitations and Future Directions

We believe that the results presented in this study are of interest as they unveil for the first time the pattern of commonalities, at both the local and the global scale, between brain connectivity networks from DWI, fMRI, and MEG. Yet we also acknowledge that the study presents some limitations, which have to be taken into account. Firstly, the computation of the whole-brain connectivity matrices required the parcellation of the brain into anatomical regions, which we have carried out with the commonly used Desikan-Killiany atlas in Freesurfer. However, it is known the definition of the ROIs influences greatly network topographies [Zalesky et al., 2010]. In multimodal approaches a consensus between modalities specific limitations must be achieved in the selection of a specific parcellation scheme. We decided to use the Desikan-Killiany atlas to be consistent with previous multimodal literature [Hagmann et al., 2008; Honey et al., 2009]. Although this atlas is low-resolution (66 regions), recently, a method to boost the resolution of this atlas, while preserving anatomical specificity was proposed [Cammoun et al., 2012]. This solution also equalizes regional volumes, avoiding bias related to differences in volume across regions. However, we decided to maintain the low-resolution atlas (66 regions), as we considered that MEG source reconstruction would not be sensitive enough to solve higher resolutions. Future work will aim to evaluate how multimodal similarities in connectivity are constrained by differences in volume between nodes. Data-driven parcellations [Varoquaux and Craddock, 2013] represent a valuable alternative that should also be evaluated to explore the atlas' influence on the network similarities.

Secondly, the MEG-FC computation requires some assumptions, to solve the ill-posed inverse problem and to estimate FC between ROIs. We employed beamforming because it has been successfully applied and recommended for the analysis of resting-state MEG-FC in several previous studies [Brookes et al., 2011a,b; Hillebrand et al., 2005, 2012; Hipp et al., 2012; Schoffelen and Gross, 2009], despite the method itself assumes that source activations are uncorrelated. Besides, we selected amplitude correlation as the connectivity metric to assess FC, which has been found to reproduce decently fMRI resting state networks [Brookes et al., 2011a,b; Maldjian et al., 2014], and included recent recommendations for leakage correction [Brookes et al., 2012; Maldjian et al., 2014]. Thirdly, it has been recently argued that fMRI time-series lasting about thirty minutes are required to achieve stability in resting-state FC [Laumann et al., 2015]. However, this is not practical in most of the MR protocols, and although traditionally, most of the research on this field has been carried out using acquisitions lengths similar to the one employed in this study, the benefits of employing longer exams are now evident [Birn et al., 2013; Laumann et al., 2015]. The same concern might be applied to the MEG data; however, to date we are not aware of any publication studying how resting-state MEG acquisition lengths relate to MEG-FC reliability. Further analyses must aim at studying the effect of acquisition lengths in the observed between modality similarities.

We must also point out that this study focuses on two topological scales, namely microscale (node similarity and hubness) and macroscale (distances between networks). However there is another scale, the mesoscale, which refers to the modular architecture of a network. It has been proved that the modular architecture in SC networks explains fMRI-FC [Betzel et al., 2014b], and therefore, we consider that our multimodal study could benefit from this mesoscale perspective. However, for the sake of representability, this was left out of this particular work.

Significant correlations between SC and fMRI-FC had been reported before: using the same parcellation scheme as in here: Honey et al. [2009] found indeed stronger correlations between SC and fMRI-FC that reached a correlation coefficient of 0.66. Honey et al. employed deterministic tractography, which generates sparser connectomes than probabilistic tractography. This may lead, when discarding zero structural connections, to higher correlations, and may explain our results. Finally, a small sample of subjects was available for this study. Future studies with larger sample sizes should be carried out to validate the present results. In particular, the Human Connectome Project plans to release a large dataset of multimodal data[1] [Van Essen et al., 2012], which will provide a unique opportunity to test our results on the similarity between SC and resting-state fMRI-FC and MEG-FC, as well as to analyze whether these similarities change with different cognitive tasks . It would be interesting as well to test whether SC influences the test-retest reliability of fMRI-FC and MEG-FC estimates.

[1]https://db.humanconnectome.org. As of February, 2015, some of these data have been already released

CONCLUSIONS

Recently, the number of multimodal neuroimaging studies has notably increased. However descriptive studies, indicating how single modal connectivity complements information on other modalities, or to what extent they are reflecting the same neuronal event are lacking. Here, we performed a thorough description on multimodal connectivity and we obtained several key findings. First, SC, fMRI-FC, and theta to gamma MEG-FC were similar, especially for regions of the DMN. Second, regions with highest similarity exhibited generally also highest hubness. Finally, distance biased SC and FC. This bias generated some spurious resemblance between modalities, but did not account for it. Altogether, this study, which combines for the first time connectivity with DWI, MEG, and fMRI in the same sample of subjects, highlights that these modalities are complementary, and thus it provides a useful ground for the design of multimodal imaging studies.

ACKNOWLEDGMENT

The authors declare that there are no conflicts of interest.

REFERENCES

Achard S, Salvador R, Whitcher B, Suckling J, Bullmore E (2006): A resilient, low-frequency, small-world human brain functional network with highly connected association cortical hubs. J Neurosci 26:63–72.

Alexander-Bloch A, Raznahan A, Bullmore E, Giedd J (2013): The convergence of maturational change and structural covariance in human cortical networks. J Neurosci 33:2889–2899.

Behrens TEJ, Berg HJ, Jbabdi S, Rushworth MFS, Woolrich M (2007): Probabilistic diffusion tractography with multiple fibre orientations: What can we gain? Neuroimage 34:144–155.

Benjamini Y, Yekutieli D (2001): The control of the false discovery rate in multiple testing under dependency. Ann Stat 29:1165–1188.

Betzel RF, Byrge L, He Y, Goñi J, Zuo XN, Sporns O (2014a): Changes in structural and functional connectivity among resting-state networks across the human lifespan. Neuroimage 102:345–357.

Betzel RF, Griffa A, Avena-Koenigsberger A, Goñi J, Thiran JP, Hagmann P, Sporns O (2014b): Multi-scale community organization of the human structural connectome and its relationship with resting-state functional connectivity. Netw Sci 1:353–373.

Birn RM, Molloy EK, Patriat R, Parker T, Meier TB, Kirk GR, Nair VA, Meyerand ME, Prabhakaran V (2013): The effect of scan length on the reliability of resting-state fMRI connectivity estimates. Neuroimage 83:550–558.

Brookes MJ, Hale JR, Zumer JM, Stevenson CM, Francis ST, Barnes GR, Owen JP, Morris PG, Nagarajan SS (2011a):

Measuring functional connectivity using MEG: Methodology and comparison with fcMRI. Neuroimage 56:1082–1104.
Brookes MJ, Woolrich M, Luckhoo H, Price D, Hale JR, Stephenson MC, Barnes GR, Smith SM, Morris PG (2011b): Investigating the electrophysiological basis of resting state networks using magnetoencephalography. Proc Natl Acad Sci USA 108:16783–16788.
Brookes MJ, Woolrich MW, Barnes GR (2012): Measuring functional connectivity in MEG: A multivariate approach insensitive to linear source leakage. Neuroimage 63:910–920.
Bullmore E, Sporns O (2009): Complex brain networks: Graph theoretical analysis of structural and functional systems. Nat Rev Neurosci 10:186–198.
Buzsaki G (2006): Rhythms of the Brain. Oxford University Press.
Cabral J, Luckhoo H, Woolrich M, Joensson M, Mohseni H, Baker A, Kringelbach ML, Deco G (2014): Exploring mechanisms of spontaneous functional connectivity in MEG: How delayed network interactions lead to structured amplitude envelopes of band-pass filtered oscillations. Neuroimage 90:423–435.
Cammoun L, Gigandet X, Meskaldji D, Thiran JP, Sporns O, Do KQ, Maeder P, Meuli R, Hagmann P (2012): Mapping the human connectome at multiple scales with diffusion spectrum MRI. J Neurosci Methods 203:386–397.
Chu CJ, Tanaka N, Diaz J, Edlow BL, Wu O, Hämäläinen M, Stufflebeam S, Cash SS, Kramer Ma (2014): EEG functional connectivity is partially predicted by underlying white matter connectivity. Neuroimage 108:23–33.
Dale A, Liu A, Fischl B, Buckner R (2000): Dynamic statistical parametric mapping: Combining fMRI and MEG for high-resolution imaging of cortical activity. Neuron 26:55–67.
De Pasquale F, Della Penna S, Snyder AZ, Lewis C, Mantini D, Marzetti L, Belardinelli P, Ciancetta L, Pizzella V, Romani GL, Corbetta M (2010): Temporal dynamics of spontaneous MEG activity in brain networks. Proc Natl Acad Sci USA 107:6040–6045.
Deco G, Jirsa VK, McIntosh AR (2011): Emerging concepts for the dynamical organization of resting-state activity in the brain. Nat Rev Neurosci 12:43–56.
Desikan RS, Ségonne F, Fischl B, Quinn BT, Dickerson BC, Blacker D, Buckner RL, Dale AM, Maguire RP, Hyman BT, Albert MS, Killiany RJ (2006): An automated labeling system for subdividing the human cerebral cortex on MRI scans into gyral based regions of interest. Neuroimage 31:968–980.
Fischl B, Van Der Kouwe A, Destrieux C, Halgren E, Ségonne F, Salat DH, Busa E, Seidman LJ, Goldstein J, Kennedy D, Caviness V, Makris N, Rosen B, Dale AM (2004): Automatically parcellating the human cerebral cortex. Cereb Cortex 14: 11–22.
Fox MD, Snyder AZ, Zacks JM, Raichle ME (2006): Coherent spontaneous activity accounts for trial-to-trial variability in human evoked brain responses. Nat Neurosci 9:23–25.
Glover GH, Li TQ, Ress D (2000): Image-based method for retrospective correction of physiological motion effects in fMRI: RETROICOR. Magn Reson Med 44:162–167.
Goñi J, van den Heuvel MP, Avena-Koenigsberger A, Velez de Mendizabal N, Betzel RF, Griffa A, Hagmann P, Corominas-Murtra B, Thiran JP, Sporns O (2014): Resting-brain functional connectivity predicted by analytic measures of network communication. Proc Natl Acad Sci USA 111:833–838.
Goshtasby AA (2012): Image registration. Advances in Computer Vision and Pattern Recognition, Advances in Pattern Recognition. London: Springer London. pp. 7–66.
Gray CM, König P, Engel AK, Singer W (1989): Oscillatory responses in cat visual cortex exhibit inter-columnar synchronization which reflects global stimulus properties. Nature 338:334–337.
Greicius MD, Krasnow B, Reiss AL, Menon V (2003): Functional connectivity in the resting brain: A network analysis of the default mode hypothesis. Proc Natl Acad Sci USA 100: 253–258.
Greicius MD, Supekar K, Menon V, Dougherty RF (2009): Resting-state functional connectivity reflects structural connectivity in the default mode network. Cereb Cortex 19:72–78.
Hagmann P, Cammoun L, Gigandet X, Meuli R, Honey CJ, Wedeen VJ, Sporns O (2008): Mapping the structural core of human cerebral cortex. PLoS Biol 6:e159.
Hämäläinen M, Hari R, Ilmoniemi RJ, Knuutila J, Lounasmaa OV (1993): Magnetoencephalography—Theory, instrumentation, and applications to noninvasive studies of the working human brain. Rev Mod Phys 65:413–497.
Hermundstad AM, Bassett DS, Brown KS, Aminoff EM, Clewett D, Freeman S, Frithsen A, Johnson A, Tipper CM, Miller MB, Grafton ST, Carlson JM (2013): Structural foundations of resting-state and task-based functional connectivity in the human brain. Proc Natl Acad Sci USA 110:6169–6174.
Hillebrand A, Barnes GR, Bosboom JL, Berendse HW, Stam CJ (2012): Frequency-dependent functional connectivity within resting-state networks: An atlas-based MEG beamformer solution. Neuroimage 59:3909–3921.
Hillebrand A, Singh KD, Holliday IE, Furlong PL, Barnes GR (2005): A new approach to neuroimaging with magnetoencephalography. Hum Brain Mapp 25:199–211.
Hinne M, Ambrogioni L, Janssen RJ, Heskes T, van Gerven MaJ (2014): Structurally-informed Bayesian functional connectivity analysis. Neuroimage 86:294–305.
Hipp JF, Hawellek DJ, Corbetta M, Siegel M, Engel AK (2012): Large-scale cortical correlation structure of spontaneous oscillatory activity. Nat Neurosci 15:884–890.
Hirschberger M, Qi Y, Steuer RE (2007): Randomly generating portfolio-selection covariance matrices with specified distributional characteristics. Eur J Oper Res 177:1610–1625.
Honey CJ, Sporns O, Cammoun L, Gigandet X, Thiran JP, Meuli R, Hagmann P (2009): Predicting human resting-state functional connectivity. Proc Natl Acad Sci USA 106:2035–2040.
Horn A, Ostwald D, Reisert M, Blankenburg F (2013): The structural-functional connectome and the default mode network of the human brain. Neuroimage 102:142–151.
Jbabdi S, Johansen-Berg H (2011): Tractography: Where do we go from here? Brain Connect 1:169–183.
Johnston JM, Vaishnavi SN, Smyth MD, Zhang D, He BJ, Zempel JM, Shimony JS, Snyder AZ, Raichle ME (2008): Loss of resting interhemispheric functional connectivity after complete section of the corpus callosum. J Neurosci 28:6453–6458.
Khalsa S, Mayhew SD, Chechlacz M, Bagary M, Bagshaw AP (2014): The structural and functional connectivity of the posterior cingulate cortex: Comparison between deterministic and probabilistic tractography for the investigation of structure–function relationships. Neuroimage 102:118–127.
Knyazev GG (2012): EEG delta oscillations as a correlate of basic homeostatic and motivational processes. Neurosci Biobehav Rev 36:677–695.
Laufs H, Krakow K, Sterzer P, Eger E, Beyerle A, Salek-Haddadi A, Kleinschmidt A (2003): Electroencephalographic signatures of attentional and cognitive default modes in spontaneous brain activity fluctuations at rest. Proc Natl Acad Sci USA 100: 11053–11058.

Laumann TO, Gordon EM, Adeyemo B, Snyder AZ, Joo SJ, Chen MY, Gilmore AW, McDermott KB, Nelson SM, Dosenbach NUF, Schlaggar BL, Mumford JA, Poldrack RA, Petersen SE (2015): Functional system and areal organization of a highly sampled individual human brain. Neuron 87:657–670.

Logothetis NK (2003): The underpinnings of the BOLD functional magnetic resonance imaging signal. J Neurosci 23:3963–3971.

Lopes da Silva, F (2010). Electrophysiological basis of MEG signals. In: Hansen PC, Kringelbach ML, Salmelin R, editors. MEG: An Introduction to Methods. Oxford University Press, pp. 1–23.

Lopes da Silva F (2013): EEG and MEG: Relevance to neuroscience. Neuron 80:1112–1128.

Luckhoo H, Hale JR, Stokes MG, Nobre AC, Morris PG, Brookes MJ, Woolrich MW (2012): Inferring task-related networks using independent component analysis in magnetoencephalography. Neuroimage 62:530–541.

Maldjian JA, Davenport EM, Whitlow CT (2014): Graph theoretical analysis of resting-state MEG data: Identifying interhemispheric connectivity and the default mode. Neuroimage 96:88–94.

Maslov S, Sneppen K (2002): Specificity and stability in topology of protein networks. Science 296:910–913.

Mesulam, M (2010): Principles of Behavioral and Cognitive Neurology, 2nd ed. New York: Oxford UP.

Mukamel R, Gelbard H, Arieli A, Hasson U (2005): Coupling between neuronal firing, field potentials, and fmri in human auditory cortex. Science 309:951–954.

Ogawa S, Tank DW, Menon R, Ellermann JM, Kim SG, Merkle H, Ugurbil K (1992): Intrinsic signal changes accompanying sensory stimulation: Functional brain mapping with magnetic resonance imaging. Proc. Natl Acad Sci USA 89:5951–5955.

Oostenveld R, Fries P, Maris E, Schoffelen JM (2011): FieldTrip: Open source software for advanced analysis of MEG, EEG, and invasive electrophysiological data. Comput Intell Neurosci 2011:156869

Papo D, Zanin M, Pineda-Pardo JA, Boccaletti S, Buldú JM (2014): Functional brain networks: Great expectations, hard times and the big leap forward. Philos Trans R Soc Lond B Biol Sci 369: 20130525

Pineda-Pardo JA, Bruña R, Woolrich M, Marcos A, Nobre K, Maestú F, Vidaurre D (2014): Guiding functional connectivity estimation by structural connectivity in MEG: An application to discrimination of mild cognitive impaired conditions. Neuroimage 101:765–777.

Power JD, Cohen AL, Nelson SM, Wig GS, Barnes KA, Church JA, Vogel AC, Laumann TO, Miezin FM, Schlaggar BL, Petersen SE (2011): Functional network organization of the human brain. Neuron 72:665–678.

Quigley M, Cordes D, Turski P, Moritz C, Haughton V, Seth R, Meyerand ME (2003): Role of the corpus callosum in functional connectivity. AJNR Am J Neuroradiol 24:208–212.

Raichle ME, Snyder AZ (2007): A default mode of brain function: A brief history of an evolving idea. Neuroimage 37:1083–1090.

Roelfsema PR, Engel AK, König P, Singer W (1997): Visuomotor integration is associated with zero time-lag synchronization among cortical areas. Nature 385:157–161.

Rubinov M, Sporns O (2010): Complex network measures of brain connectivity: Uses and interpretations. Neuroimage 52:1059–1069.

Schoffelen JM, Gross J (2009): Source connectivity analysis with MEG and EEG. Hum Brain Mapp 30:1857–1865.

Shen X, Tokoglu F, Papademetris X, Constable RT (2013): Groupwise whole-brain parcellation from resting-state fMRI data for network node identification. Neuroimage 82:403–415.

Singer W, Gray CM (1995): Visual feature integration and the temporal correlation hypothesis. Annu Rev Neurosci 18:555–586.

Singh KD (2012): Which "neural activity" do you mean? fMRI, MEG, oscillations and neurotransmitters. Neuroimage 62:1121–1130.

Skudlarski P, Jagannathan K, Calhoun VD, Hampson M, Skudlarska BA, Pearlson G (2008): Measuring brain connectivity: Diffusion tensor imaging validates resting state temporal correlations. Neuroimage 43:554–561.

Smith SM (2002): Fast robust automated brain extraction. Hum Brain Mapp 17:143–155.

Taulu S, Simola J (2006): Spatiotemporal signal space separation method for rejecting nearby interference in MEG measurements. Phys Med Biol 51:1759–1768.

Tewarie P, Hillebrand a, van Dellen E, Schoonheim MM, Barkhof F, Polman CH, Beaulieu C, Gong G, van Dijk BW, Stam CJ (2014): Structural degree predicts functional network connectivity: A multimodal resting-state fMRI and MEG study. Neuroimage 97:296–307.

Tzourio-Mazoyer N, Landeau B, Papathanassiou D, Crivello F, Etard O, Delcroix N, Mazoyer B, Joliot M (2002): Automated anatomical labeling of activations in SPM using a macroscopic anatomical parcellation of the MNI MRI single-subject brain. Neuroimage 15:273–289.

Van den Heuvel MP, Mandl RCW, Kahn RS, Hulshoff Pol HE (2009): Functionally linked resting-state networks reflect the underlying structural connectivity architecture of the human brain. Hum Brain Mapp 30:3127–3141.

Van Dijk KRa, Sabuncu MR, Buckner RL (2012): The influence of head motion on intrinsic functional connectivity MRI. Neuroimage 59:431–438.

Van Essen DC, Ugurbil K, Auerbach E, Barch D, Behrens TEJ, Bucholz R, Chang A, Chen L, Corbetta M, Curtiss SW, Della Penna S, Feinberg D, Glasser MF, Harel N, Heath AC, Larson-Prior L, Marcus D, Michalareas G, Moeller S, Oostenveld R, Petersen SE, Prior F, Schlaggar BL, Smith SM, Snyder AZ, Xu J, Yacoub E (2012): The Human Connectome Project: A data acquisition perspective. Neuroimage 62:2222–2231.

Van Veen BD, van Drongelen W, Yuchtman M, Suzuki A (1997): Localization of brain electrical activity via linearly constrained minimum variance spatial filtering. IEEE Trans Biomed Eng 44:867–880.

Varoquaux G, Craddock RC (2013): Learning and comparing functional connectomes across subjects. Neuroimage 80:405–415.

Vértes PE, Alexander-Bloch AF, Gogtay N, Giedd JN, Rapoport JL, Bullmore ET (2012): Simple models of human brain functional networks. Proc Natl Acad Sci USA 109:5868–5873.

Yeo BTT, Krienen FM, Sepulcre J, Sabuncu MR, Lashkari D, Hollinshead M, Roffman JL, Smoller JW, Zöllei L, Polimeni JR, Fischl B, Liu H, Buckner RL (2011): The organization of the human cerebral cortex estimated by intrinsic functional connectivity. J Neurophysiol 106:1125–1165.

Zalesky A, Fornito A, Harding IH, Cocchi L, Yücel M, Pantelis C, Bullmore ET (2010): Whole-brain anatomical networks: does the choice of nodes matter? Neuroimage 50:970–983.

Zalesky A, Fornito A, Bullmore E (2012): On the use of correlation as a measure of network connectivity. Neuroimage 60:2096–2106.

Zumer JM, Brookes MJ, Stevenson CM, Francis ST, Morris PG (2010): Relating BOLD fMRI and neural oscillations through convolution and optimal linear weighting. Neuroimage 49: 1479–1489.